Supporting information

Coupling PtZn intermetallic and atomically dispersed cobalt towards efficient and stable oxygen reduction reaction catalysts

Lei Zhao [a], Xueqiang Qi [b,c,*], Tingting Yang [c], Pei Xiong [a], Xiaobin Niu [a], Jinxia Jiang [d], Qian Xue [c], Le Yu [e], Jun Song Chen [a,f,g], Andreu Cabot [b,h,*], and Rui Wu [a,*]

[a] School of Materials and Energy, University of Electronic Science and Technology of China, Chengdu 611731, China.

[b] Catalonia Institute for Energy Research (IREC), Sant Adrià de Besòs, Barcelona 08930, Spain.

[c] College of Chemistry and Chemical Engineering, Chongqing University of Technology, Chongqing 400054, China.

[d] Chongqing Medical and Pharmaceutical College, Chongqing, 400020, China

[e] State Key Lab of Organic-Inorganic Composites, Beijing University of Chemical Technology, Beijing 100029, China.

[f] Interdisciplinary Materials Research Center, Institute for Advanced Study, Chengdu University, Chengdu 610106, China

[g] Shenzhen Institute for Advanced Study, University of Electronic Science and Technology of China, Shenzhen 518000, China.

[h] ICREA, Pg. Lluis Companys 23, Barcelona 08010, Catalonia, Spain

* Corresponding Authors

Xueqiang Qi, Email: xqqi@cqut.edu.cn; Andreu Cabot, Email: acabot@irec.cat; Rui Wu,

Email: ruiwu0904@uestc.edu.cn

Computational details

Spin-polarized DFT calculations were performed with the Vienna Ab initio Simulation Package (VASP).[1,2] The Perdew-Burke-Ernzerhof (PBE) functional within the generalized gradient approximation (GGA) was adopted to describe electronic exchange-correlation energy.[3] The ionic cores were described with the projector augmented wave (PAW) method. In all the calculations, the vacuum was established at 15 Å to create a true crystal surface. A cutoff energy of 400 eV was provided and a 3×3×1 Monkhorst Pack k-point sampling was chosen for the well-converged energy values. Geometry optimizations were pursued until the force on each atom falls below the convergence criterion of 0.02 eV/Å and energies converged within 10^{-5} eV.

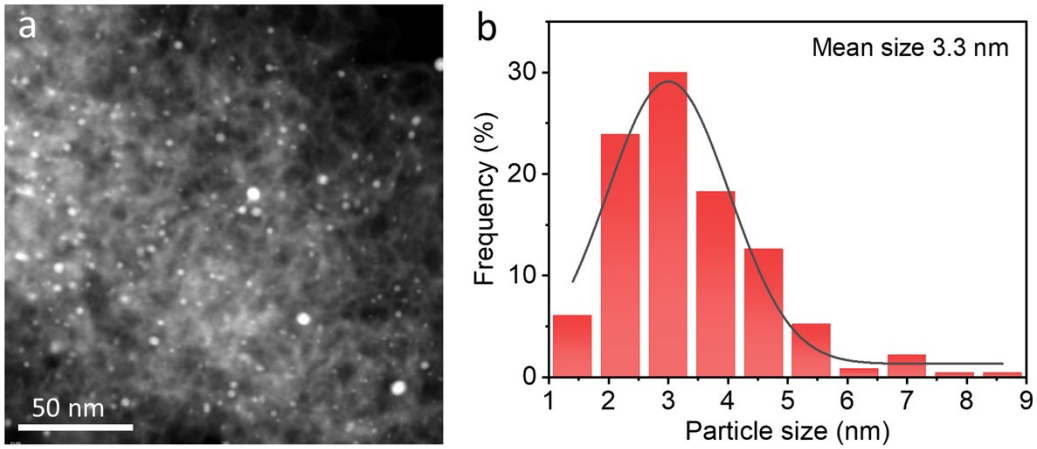

Fig. S1 (a) TEM image of PtZn-NC and (b) corresponding size distribution histogram of PtZn NPs.

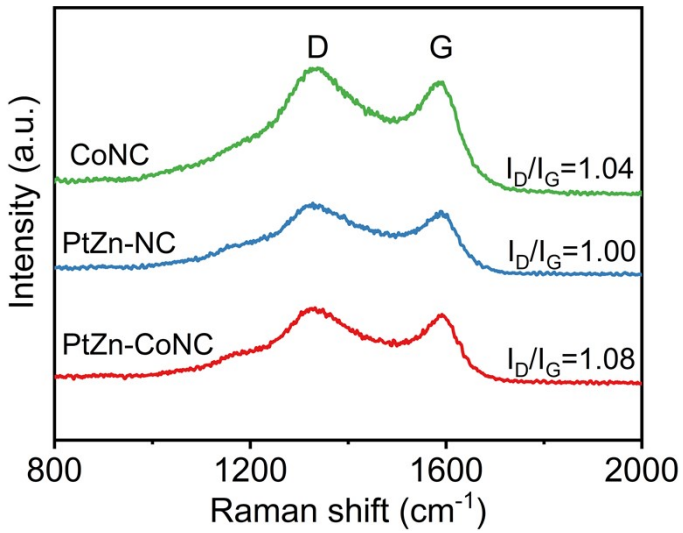

Fig. S2 Raman spectra of PtZn-CoNC, PtZn-NC and CoNC.

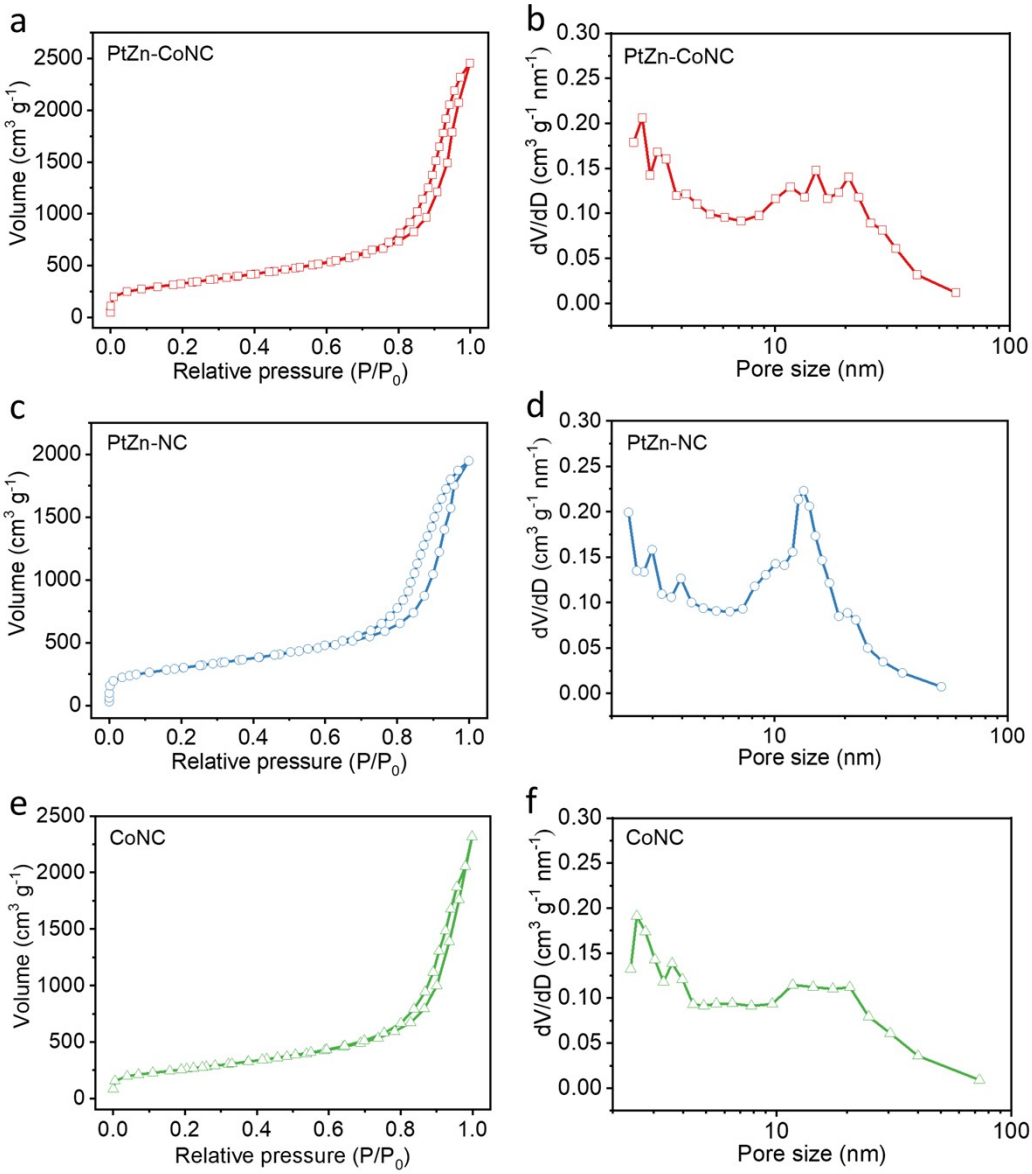

Fig. S3 N_2 adsorption/desorption isotherms and pore size distribution plots of (a, b) PtZn-CoNC, (c, d) PtZn-NC and (e, f) CoNC.

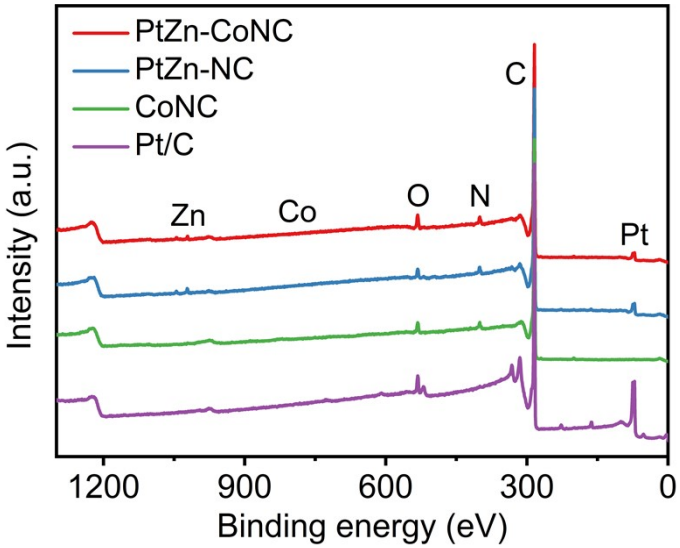

Fig. S4 XPS survey spectra of PtZn-CoNC, PtZn-NC, CoNC and Pt/C.

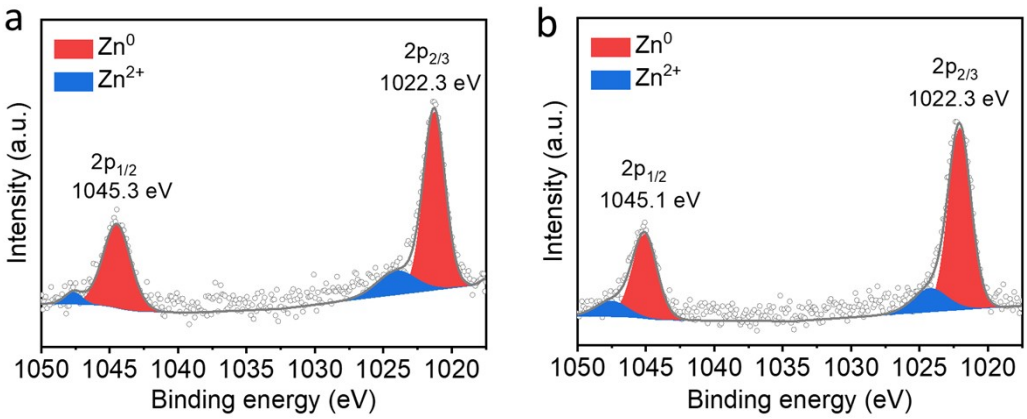

Fig. S5 Zn 2p XPS spectra of (a) PtZn-CoNC and (b) PtZn-NC.

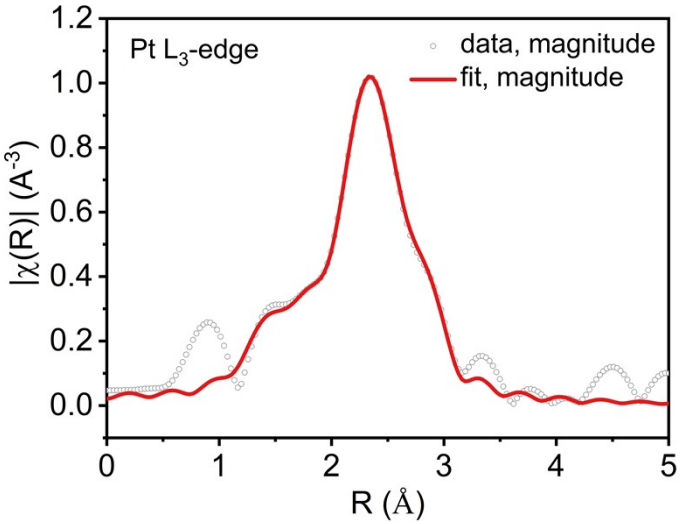

Fig. S6 Fitted Pt EXAFS spectrum of PtZn-CoNC.

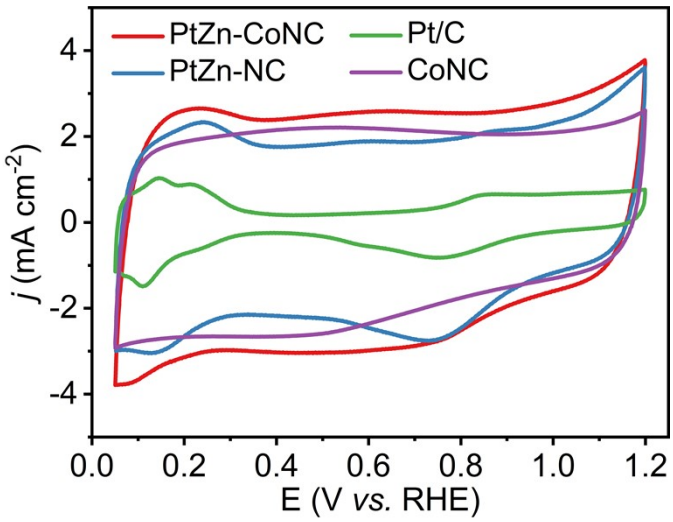

Fig. S7 CV curves for PtZn-CoNC, PtZn-NC and commercial Pt/C catalysts.

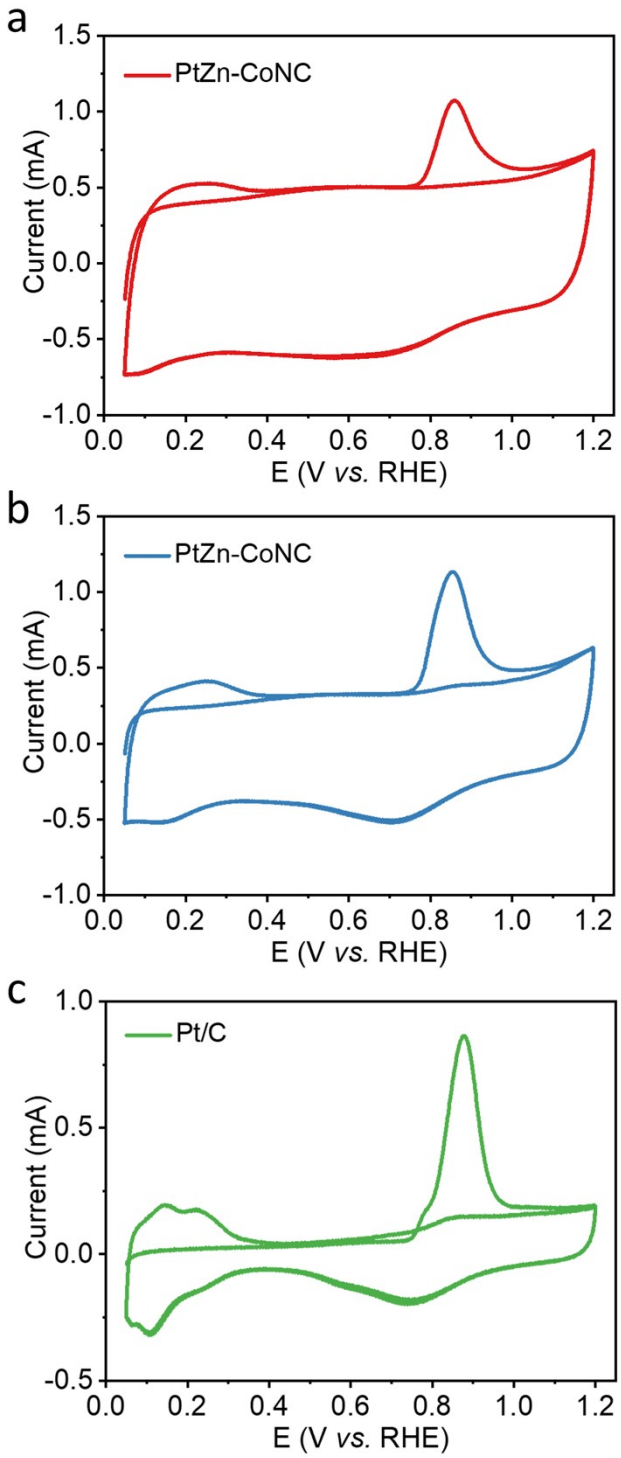

Fig. S8 CO stripping voltammograms of (a) PtZn-CoNC, (b) PtZn-NC and (c) Pt/C.

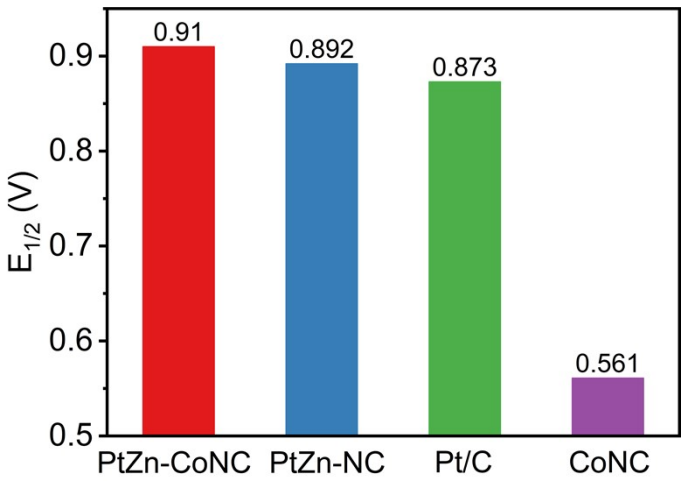

Fig. S9 Half-wave potentials for PtZn-CoNC, PtZn-NC and Pt/C.

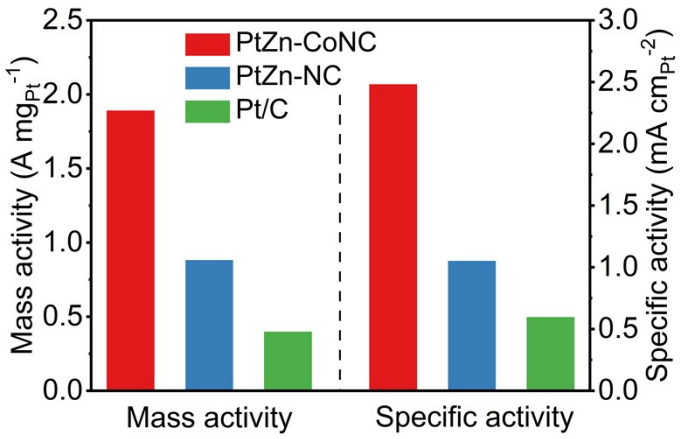

Fig. S10 Mass activities and specific activities for PtZn-CoNC, PtZn-NC and Pt/C at 0.85 V *vs.* RHE.

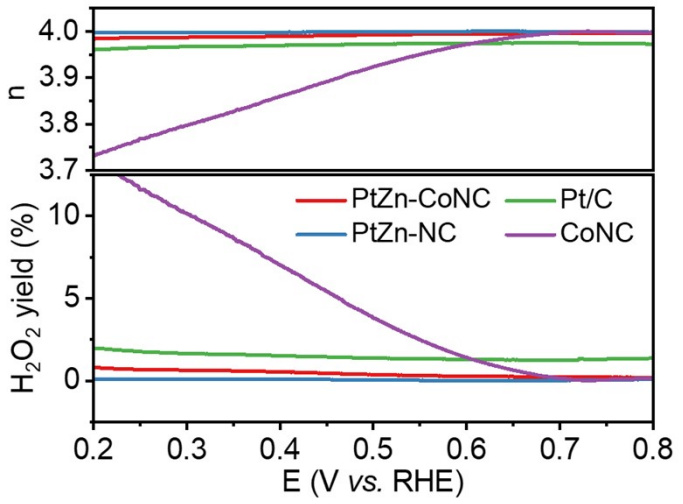

Fig. S11 Electron transfer number and H_2O_2 yield for PtZn-CoNC, PtZn-NC, Pt/C and CoNC obtained from RRDE measurements.

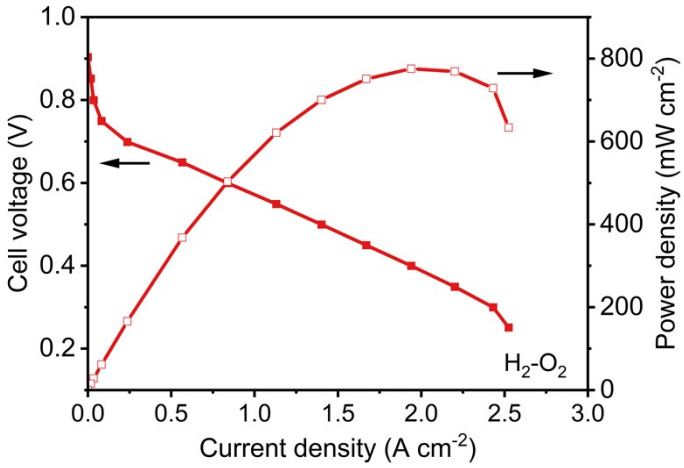

Fig. S12 Polarization and power density curves of H_2-O_2 fuel cells based on PtZn-CoNC and commercial Pt/C cathode catalysts with a cathode Pt loading of 0.05 mg cm_{Pt}^{-2}.

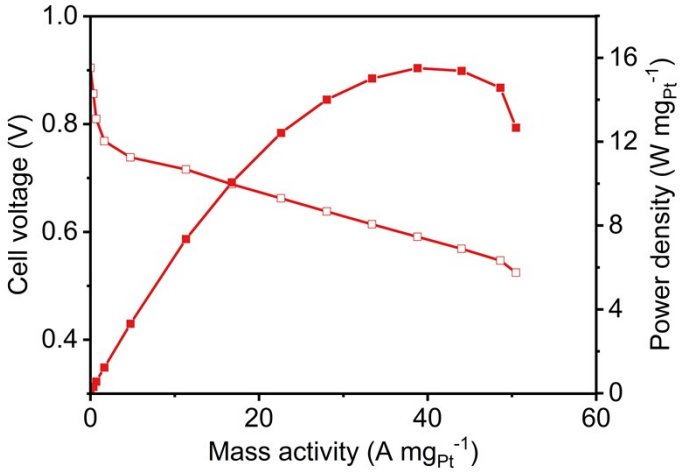

Fig. S13 Mass normalized H_2-O_2 fuel cell performance of PtZn-CoNC.

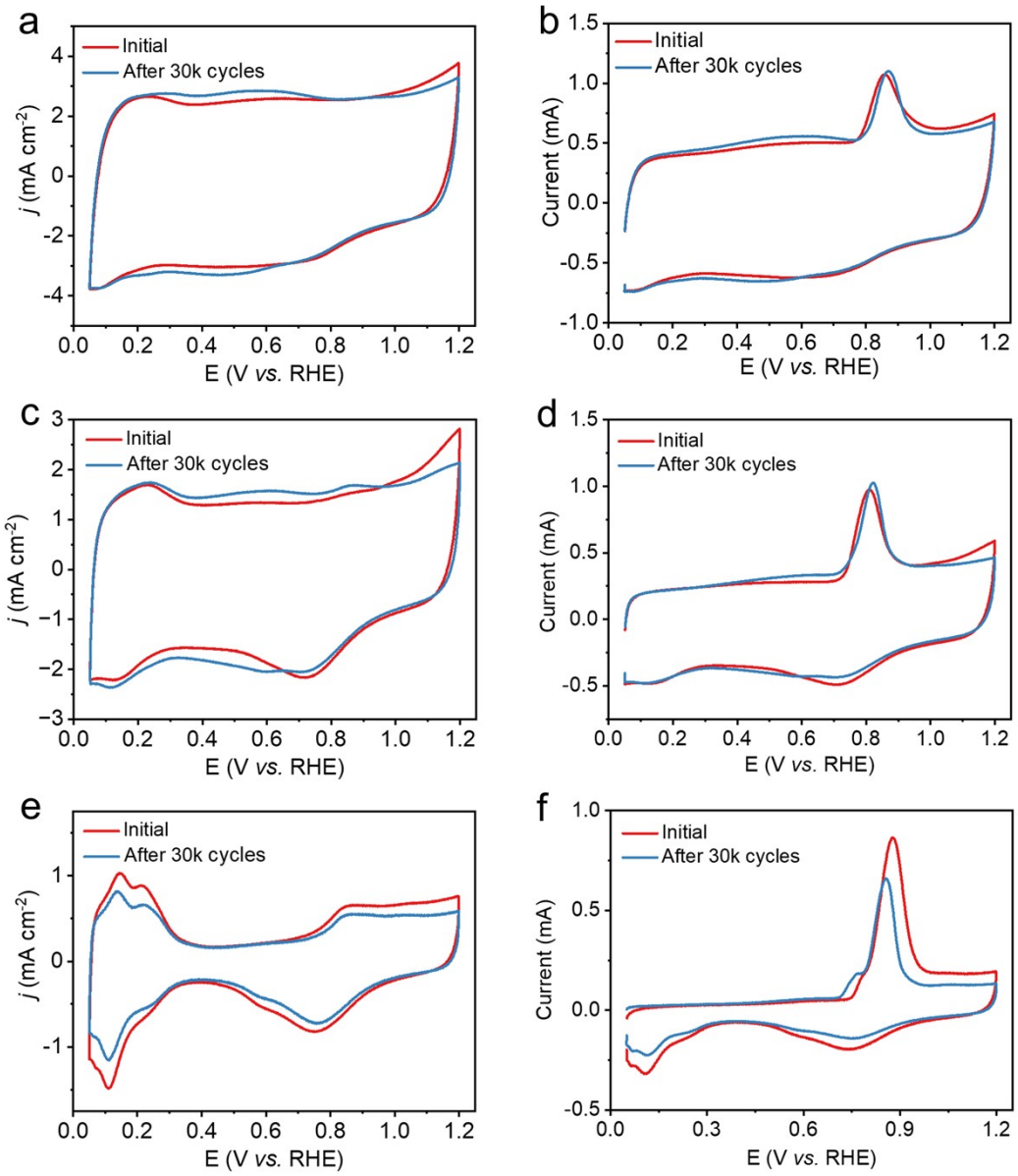

Fig. S14 CV curves and CO stripping voltammograms before and after 30,000 cycles of (a, b) PtZn-CoNC, (c, d) PtZn-NC and (e, f) Pt/C.

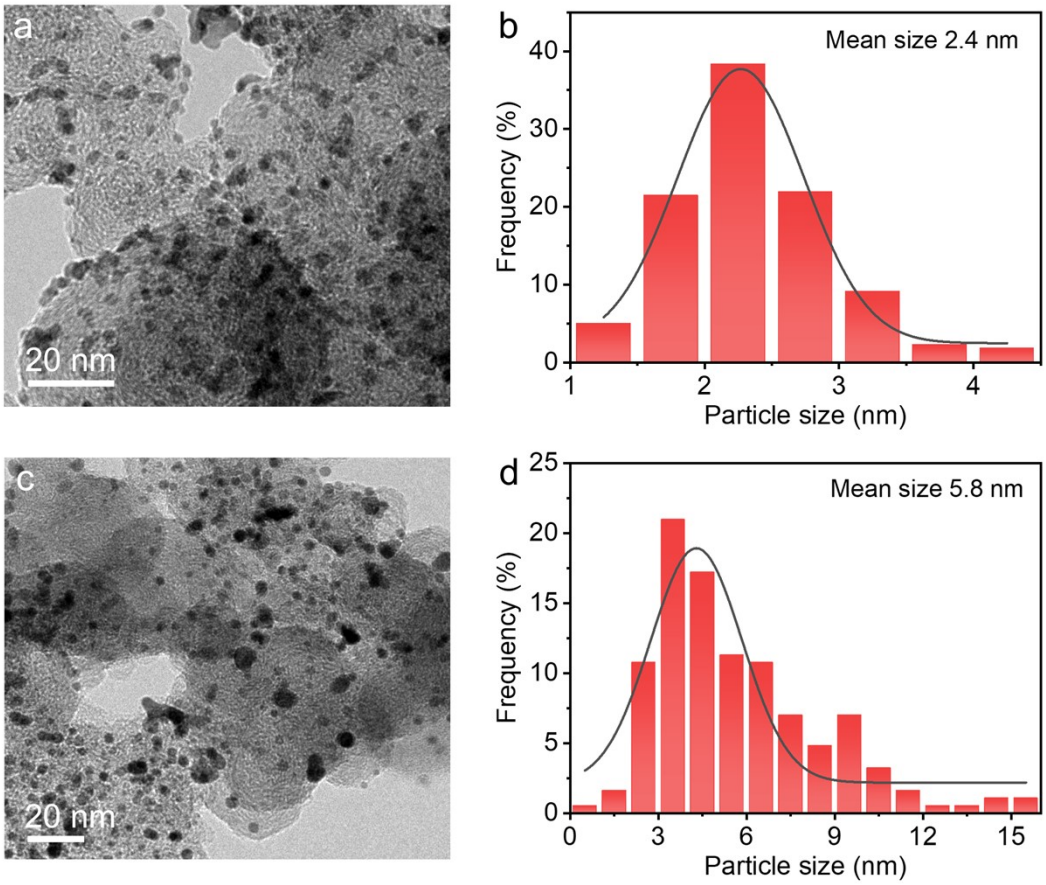

Fig. S15 TEM images and corresponding Pt size distributions of (a, b) fresh Pt/C catalyst and (c, d) aged Pt/C catalyst after 30,000 cycles.

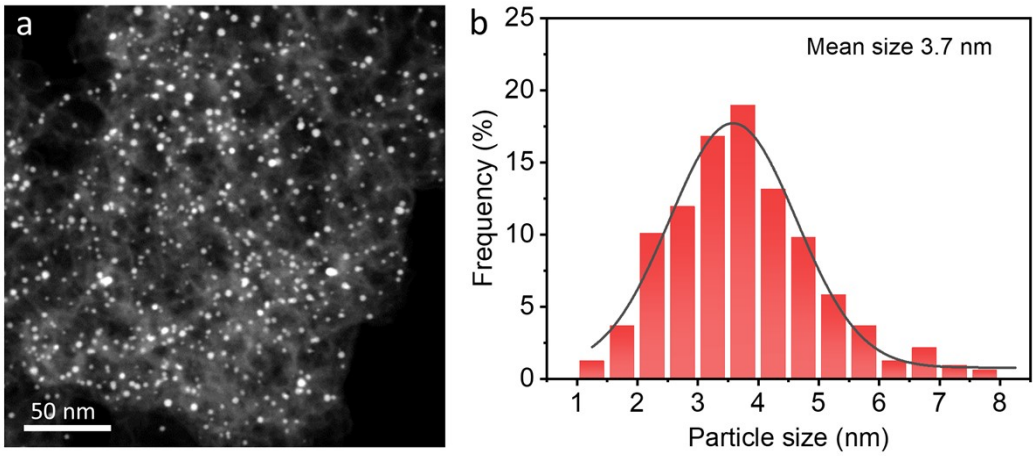

Fig. S16 (a) TEM image and (b) corresponding PtZn particle size distribution of PtZn-NC after 30,000 potential cycles.

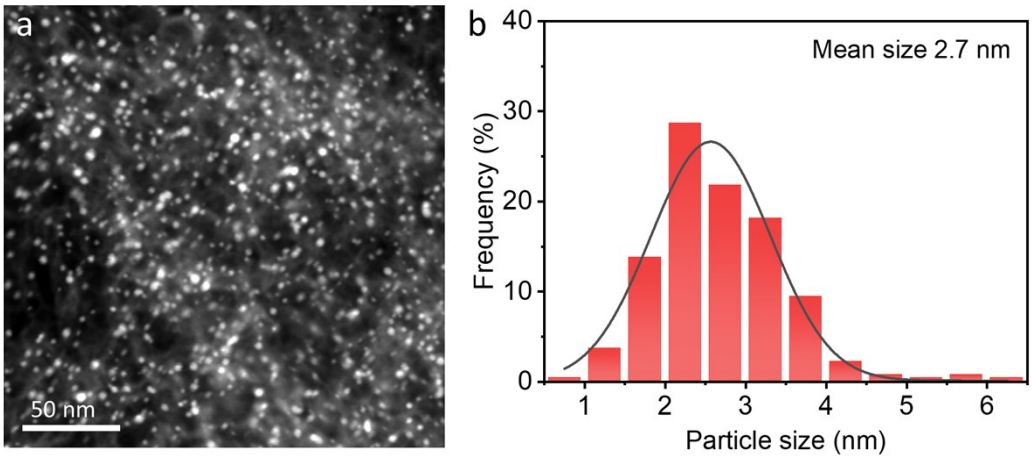

Fig. S17 (a) TEM image and (b) corresponding PtZn particle size distribution of PtZn-CoNC after 30,000 potential cycles.

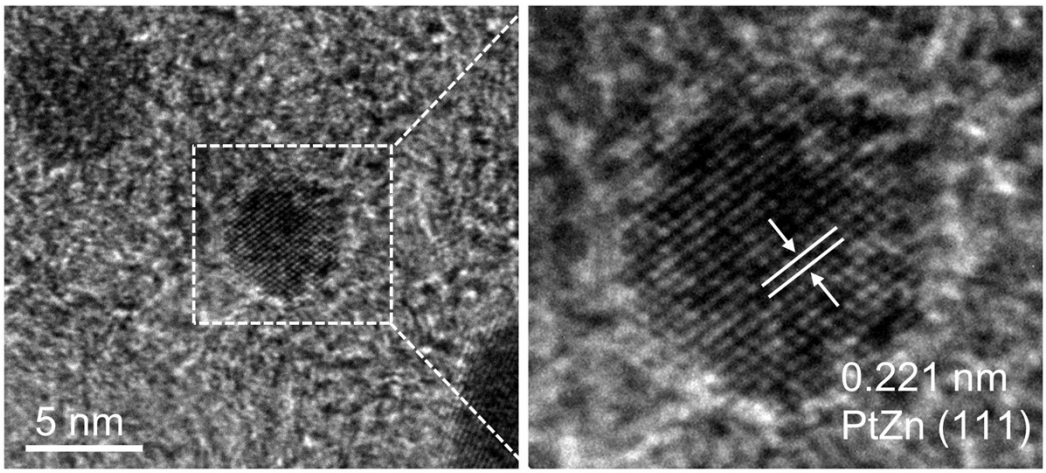

Fig. S18 HR-TEM images of PtZn-CoNC after 30,000 potential cycles.

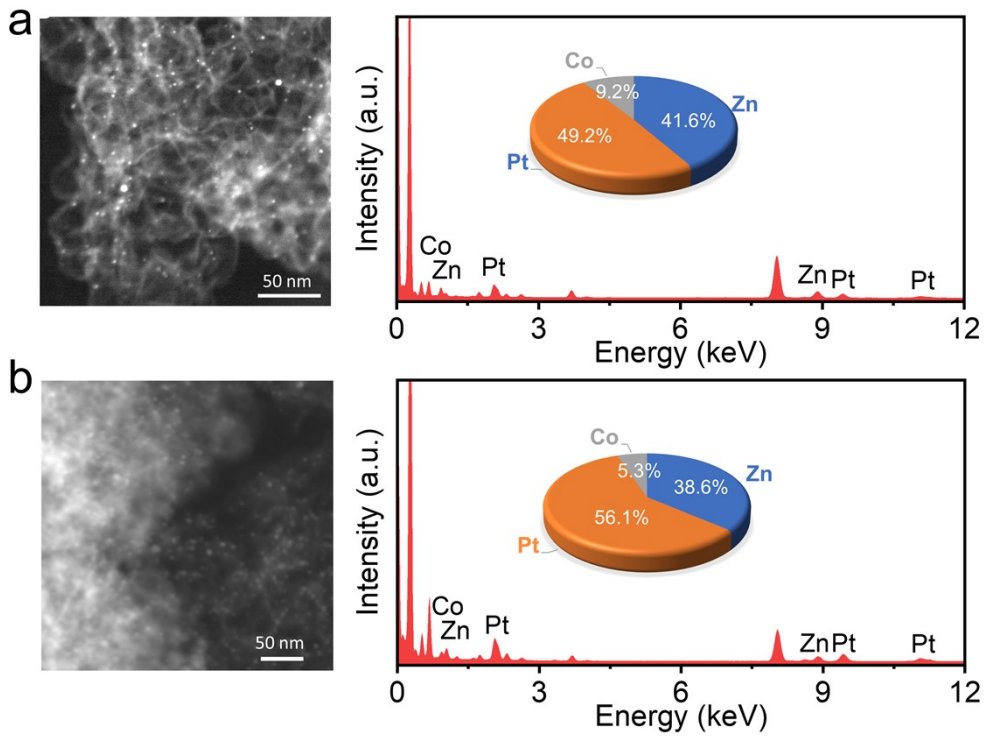

Fig. S19 TEM images and corresponding EDS analysis of PtZn-CoNC: (a) initial and (b) after the 30k cycles.

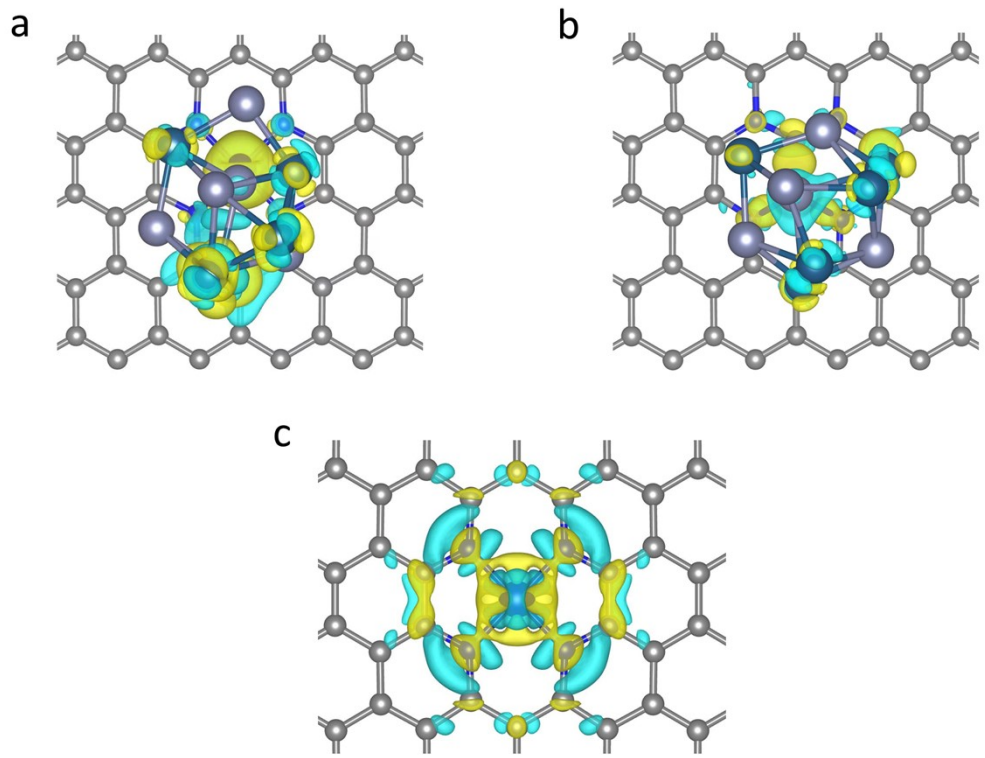

Fig. S20 Differential charge diagrams of (a) PtZn/CoN_4, (b) PtZn/NC and (c) CoN_4 at top view.

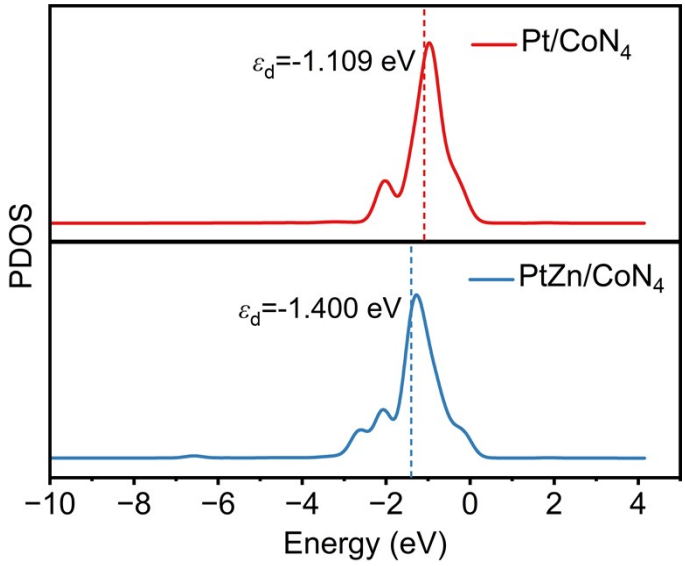

Fig. S21 Projected density of states (PDOS) diagrams of Pt in Pt/CoN_4 and $PtZn/CoN_4$.

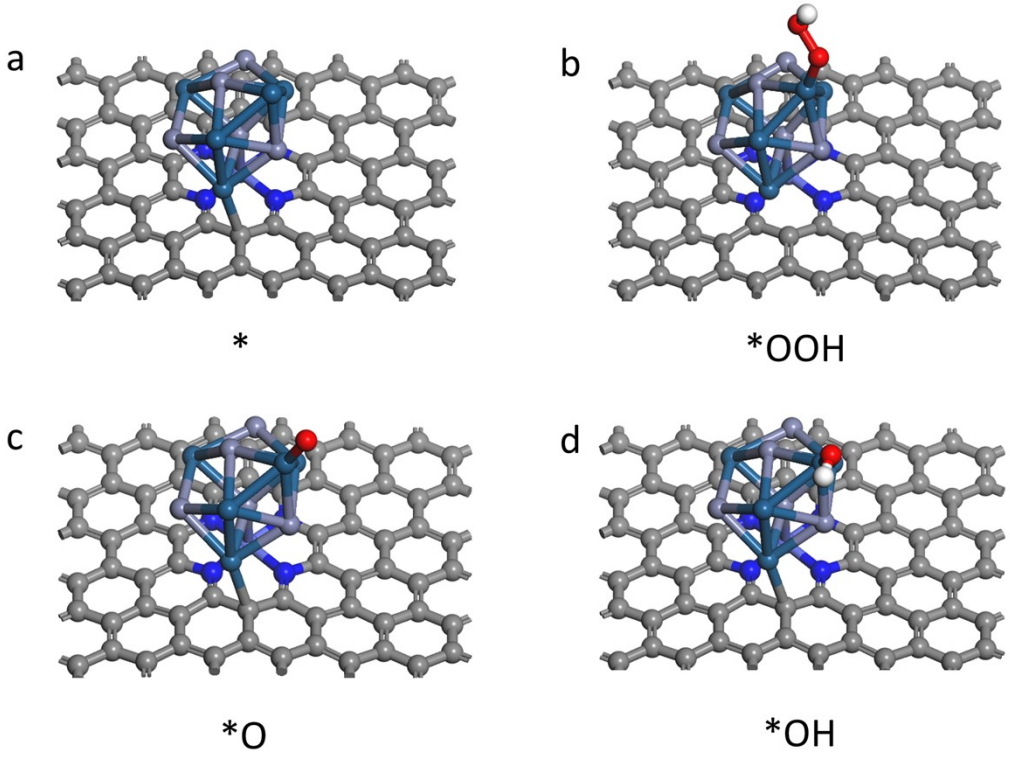

Fig. S22 Configurations of the adsorbed intermediates on $PtZn/CoN_4$: (a) bare surface (b) *OOH, (c) *O, and (d) *OH.

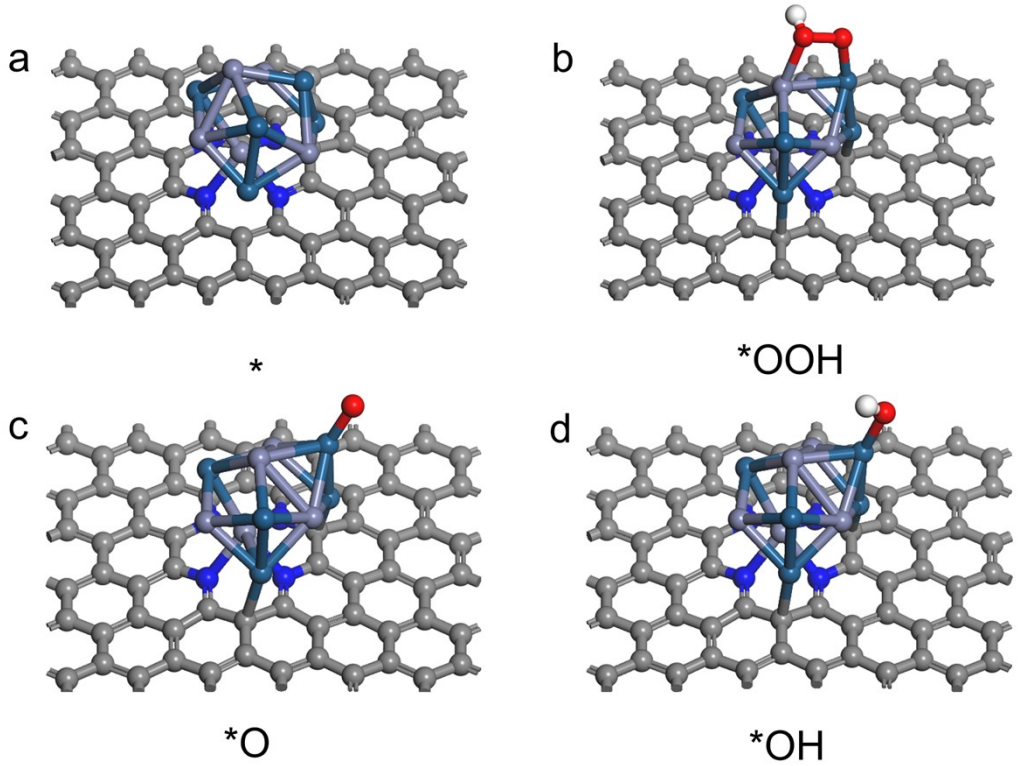

Fig. S23 Configurations of the adsorbed intermediates on PtZn/NC: (a) bare surface (b) *OOH, (c) *O, and (d) *OH.

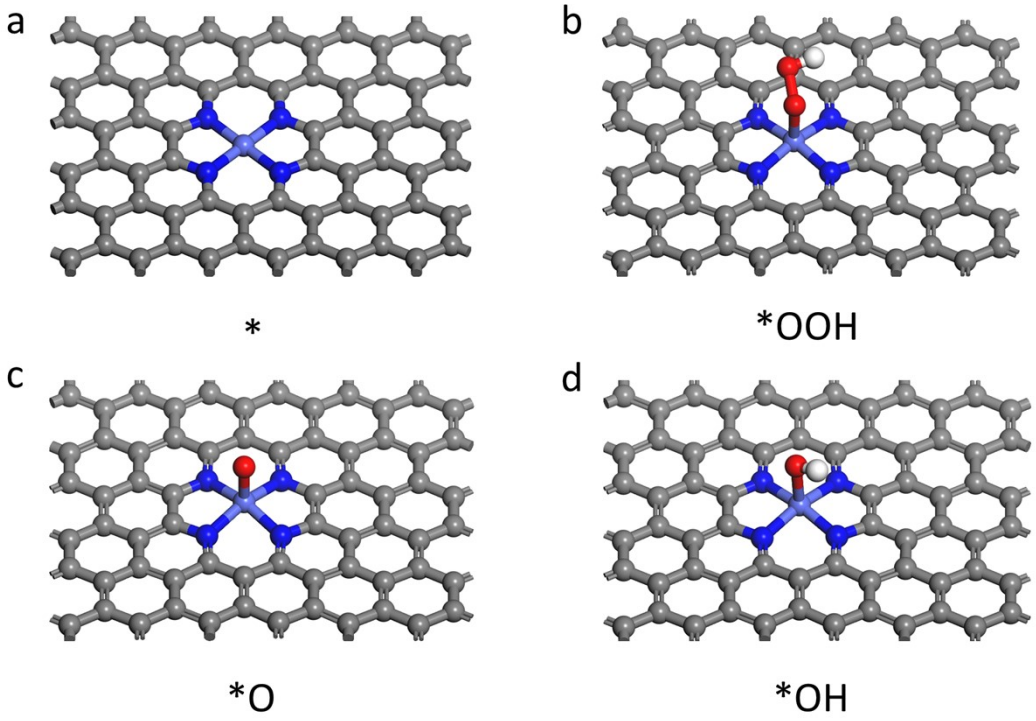

Fig. S24 Configurations of the adsorbed intermediates on CoN_4: (a) bare surface (b) *OOH, (c) *O, and (d) *OH.

Table S1 Pore parameters for PtZn-CoNC, PtZn-NC and CoNC.

Sample	PtZn-CoNC	PtZn-NC	CoNC
BET (m^2 g^{-1})	1157.6	1054.2	920.8
Average pore size (nm)	6.94	5.83	7.79
Total pore volume (cm^3 g^{-1})	4.05	5.72	3.58

Table S2 Elemental composition determined by XPS for different samples.

	C / at%	N / at%	Pt / at%	Zn / at%	Co / at%
PtZn-CoNC	93.39	5.64	0.46	0.34	0.18
PtZn-NC	95.09	4.22	0.43	0.26	--
CoNC	93.99	5.89	--	--	0.12
Pt/C	99.16	--	0.84	--	--

Table S3. The bind energies of individual peak deconvolution of Pt 4f spectra and corresponding relative concentration of Pt species in PtZn-CoNC, PtZn-NC and Pt/C samples.

Sample	Pt $4f_{7/2}$				Pt $4f_{5/2}$			
	Pt^0		Pt^{2+}		Pt^0		Pt^{2+}	
	Binding energy	Content	Binding energy	content	Binding energy	content	Binding energy	content
PtZn-CoNC	71.4 eV	30.5%	72.5 eV	19.7 %	74.9 eV	30.5%	76.0 eV	20.8%
PtZn-NC	71.5 eV	29.9%	72.6 eV	18.7%	75.0 eV	32.0%	76.2 eV	18.7%
Pt/C	71.9 eV	25.2%	72.8 eV	26.0%	75.3 eV	26.9%	76.4 eV	21.8%

Table S4 Structural parameters extracted from the EXAFS fitting of PtZn-CoNC.

Sample	Path	N	R (Å)	σ^2 ($\times10^{-3}$ Å^2)	ΔE_0 (eV)	R, %
Pt foil[a]	Pt-Pt1	12	2.75±0.01	5±1	7.6±0.3	0.43
	Pt-Pt2	6	3.88±0.02	8±2		
PtZn[b]	Pt-O	0.6±0.2	1.86±0.06	2±1	-3.0±2.3	0.77
	Pt-Zn	2.6±0.6	2.56±0.02	2±1		
	Pt-Pt	4.1±1.0	2.61±0.03	4±1		

[a]: k range: 3-14.3 (Å^{-1}); R range: 1-3.6 Å; [b]: k range: 3-12 (Å^{-1}); R range: 1-3.2 Å; S_0^2 = 0.83, S_0^2 was determined from Pt foil. The bold numbers were set as fixed coordination numbers.

Table S5 Comparison of the H_2-O_2 fuel cell performance for recently reported Pt alloy electrocatalysts.

Catalyst	**Cathode Loading (mg_{Pt} cm^{-2})**	**Peak Power Density (mW cm^{-2})**	**Peak Power Density (W mg_{Pt}^{-1})**	**MA[a] (A mg_{Pt}^{-1})**	**References**
PtZn-CoNC	**0.05**	**776**	**15.5**	**14.60[b]**	**This work**
PtCo@NGNS	0.1	860	8.6	N/A	[4]
Pt1Co1-MC@Pt/C	0.2	2300	11.5	0.46	[5]
PtCo/Co–N–C	0.05	700	12.0	10.52[c]	[6]
PtCoNi@NCNTs	0.066	700	10.2	8.11[b]	[7]
PtA@FeSA–N–C	0.13	1.31	10.1	0.45	[8]
PtNiCo/NC	0.12	1070	9.0	N/A	[9]
oh-PtNi(Mo)/C	0.1	1170	11.7	0.45	[10]

MA[a]: Single cell mass activity based on the cathodic Pt-loading at a voltage of 0.9 V, MA[b]: at a voltage of 0.7 V and MA[c]: at a voltage of 0.6 V.

N/A: not applicable

Table S6 Comparison of the ORR performance for recently reported Pt electrocatalysts.

Catalyst	$E_{1/2}$[a] (V)	MA[b] (A mg_{Pt}^{-1}) at 0.9 V	Loss of $E_{1/2}$ (mV) after ADTs[c]	Loss of MA after ADTs (%)	References
PtZn-CoNC	**0.910**	**0.44**	**5 (30k)**	**12.8 (30k)**	**This work**
Pt1Co1-IMC@Pt/C-2.5	N/A[d]	0.53	10 (30k)	23.4 (30k)	[5]
O-$PtCo_3$ @HNCS	0.909	0.54	10 (20k)	7.4 (20k)	[11]
$PtNi_3$@OMC-A	0.907	2.11 (0.85 V)	10 (10k)	20.8 (10k)	[12]
Pt-Co ND-NF	0.95	0.939	18 (5k)	39.7 (5k)	[13]
Pt/ZnFe-N-C	0.790	0.20 (0.85 V)	1 (2k)	11.3 (2k)	[14]
$PtCo/Zn_{11}Co$	0.922	0.46	N/A	~20 (60k)	[15]
O-Pt-Fe@NC/C	N/A	0.53	4 (10k)	14.1 (10k)	[16]
Pt-Co NF	N/A	0.4 (0.95 V)	N/A	15 (5k)	[17]
10%-PtZn@NC-800	0.912	0.283	1 (5k)	N/A	[18]

$E_{1/2}$[a]: half-wave potential;

MA[b]: mass activity;

ADTs[c]: accelerated durability tests

N/A[d]: not applicable.

Reference

1. G. Kresse and J. Hafner, *Phys. Rev. B*, 1993, **47**, 558–561.
2. G. Kresse and J. Furthmiiller, *Comput. Mater. Sci.*, 1996, **6**, 15–50.
3. B. Hammer, L. B. Hansen and J. K. No"rskov, *Phys. Rev. B* 1999, **59**, 7413–7421.
4. S. Zaman, Y. Q. Su, C. L. Dong, R. Qi, L. Huang, Y. Qin, Y. C. Huang, F. M. Li, B. You, W. Guo, Q. Li, S. Ding and B. Y. Xia, *Angew. Chem. Int. Ed.*, 2022, **61**, e202115835.
5. Q. Cheng, S. Yang, C. Fu, L. Zou, Z. Zou, Z. Jiang, J. Zhang and H. Yang, *Energy Environ. Sci.*, 2022, **15**, 278–286.
6. P. Guo, Y. Xia, B. Liu, M. Ma, L. Shen, Y. Dai, Z. Zhang, Z. Zhao, Y. Zhang, L. Zhao and Z. Wang, *ACS Appl Mater Interfaces*, 2022, **14**, 53819–53827.
7. S. Zaman, X. Tian, Y.-Q. Su, W. Cai, Y. Yan, R. Qi, A. I. Douka, S. Chen, B. You, H. Liu, S. Ding, X. Guo and B. Y. Xia, *Sci. Bull.*, 2021, **66**, 2207–2216.
8. X. Ao, W. Zhang, B. Zhao, Y. Ding, G. Nam, L. Soule, A. Abdelhafiz, C. Wang and M. Liu, *Energy Environ. Sci.*, 2020, **13**, 3032–3040.
9. S. Hanif, X. Shi, N. Iqbal, T. Noor, R. Anwar and A. M. Kannan, *Appl. Catal. B: Environ.*, 2019, **258**, 117947.
10. F. Dionigi, C. C. Weber, M. Primbs, M. Gocyla, A. M. Bonastre, C. Spori, H. Schmies, E. Hornberger, S. Kuhl, J. Drnec, M. Heggen, J. Sharman, R. E. Dunin-Borkowski and P. Strasser, *Nano Lett.*, 2019, **19**, 6876–6885.
11. Y. Hu, X. Guo, T. Shen, Y. Zhu and D. Wang, *ACS Catal.*, 2022, **12**, 5380–5387.
12. K. Wang, Y. Wang, S. Geng, Y. Wang and S. Song, *Adv. Funct. Mater.*, 2022, **32**, 2113399.
13. X. Zhu, L. Huang, M. Wei, P. Tsiakaras and P. K. Shen, *Appl. Catal. B: Environ.*, 2021, **281**, 119460.
14. J. Li, Q. Zhou, M. Yue, S. Chen, J. Deng, X. Ping, Y. Li, J. Li, Q. Liao, M. Shao and Z. Wei, *Appl. Catal. B: Environ.*, 2021, **284**, 119728.
15. Y. Xiong, Y. Yang, F. J. DiSalvo and H. D. Abruna, *ACS Nano*, 2020, **14**, 13069–13080.
16. Y. Hu, T. Shen, X. Zhao, J. Zhang, Y. Lu, J. Shen, S. Lu, Z. Tu, H. L. Xin and D. Wang, *Appl. Catal. B: Environ.*, 2020, **279**, 119370.
17. S. Chen, M. Li, M. Gao, J. Jin, M. A. van Spronsen, M. B. Salmeron and P. Yang, *Nano Lett.*, 2020, **20**, 1974–1979.
18. Y. Xue, H. Li, X. Ye, S. Yang, Z. Zheng, X. Han, X. Zhang, L. Chen, Z. Xie, Q. Kuang and L. Zheng, *Nano Res.*, 2019, **12**, 2490–2497.